Research Square

Preprints are preliminary reports that have not undergone peer review.
They should not be considered conclusive, used to inform clinical practice,
or referenced by the media as validated information.

# Cross-Target Docking of GPX4 and SLC7A11 Inhibitor Candidates Against FSP1 in KRAS-Mutant Colorectal Cancer: Dual and Triple Pathway Leads

**Cumhur Gokhan Ekmekci**

cgekmekci2@yahoo.com

Independent Researcher https://orcid.org/0000-0002-0967-172X

**Research Article**

**Keywords:** ferroptosis, FSP1, GPX4, SLC7A11, KRAS, dual inhibition, virtual screening, colorectal cancer, AIFM2, CoQ10

**Posted Date:** October 6th, 2026

**DOI:** https://doi.org/10.21203/rs.3.rs-11249714/v1

**License:** This work is licensed under a Creative Commons Attribution 4.0 International License. Read Full License

**Additional Declarations:** The authors declare no competing interests.

## Abstract

# Background.

Ferroptosis resistance in KRAS-mutant colorectal cancer (CRC) runs through at least two independent axes — the GPX4–glutathione pathway and the FSP1–CoQ10–NAD(P)H pathway — and KRAS-mutant cells specifically upregulate FSP1 via MAPK and NRF2. Selective inhibition of GPX4 or SLC7A11 alone leaves FSP1 resistance intact, and no single compound with dual GPX4 and FSP1 activity has been reported.

# Methods.

We ran cross-target docking of eleven compounds against the crystal structure of human FSP1 (PDB 8WIK, 2.00 Å, with 6-OH-FAD and NAD) using AutoDock Vina 1.2.7 [8], targeting the CoQ10/catalytic pocket and the NAD-binding allosteric cavity. The set comprised two GPX4 candidates (JKE-1674, ClAcNH_001) from prior docking against PDB 7KTC, one SLC7A11 candidate (PipAryl_005) from PDB 7P9U, two reference FSP1 inhibitors (iFSP1, FSEN1), and six de novo CoQ10-pharmacophore scaffolds. All compounds were profiled for Lipinski compliance, PAINS status, and ADMET in RDKit. Vertical electron affinities were computed at r2SCAN-3c/CPCM(water) in ORCA 5.0 [26] to assess the redox liability of quinone scaffolds.

# Results.

JKE-1674 (GPX4 − 8.83 kcal/mol) scored − 9.90 at the FSP1 CoQ pocket, approaching the iFSP1 reference (− 10.10). PipAryl_005 (SLC7A11 − 8.47 kcal/mol) scored − 10.60, exceeding iFSP1 at both FSP1 sites. Among the de novo scaffolds, Quinone_002 (QED 0.916, − 9.80) and CoQ_Mimic_002 (QED 0.899, − 9.20) ranked highest. Quantum-chemical calculations confirmed that naphthoquinone scaffolds have electron affinities within the CoQ0 substrate range, validating their quinone_A PAINS flags; the dimethoxybenzene CoQ_Mimic_001 (EA 1.26 eV) is redox-inert. Four PAINS-clean, Lipinski-compliant compounds were advanced as priority candidates.

# Conclusions.

JKE-1674 and PipAryl_005 carry in silico dual GPX4–FSP1 and triple SLC7A11–FSP1 profiles against the experimental 8WIK receptor, both with better drug-likeness than iFSP1. FSP1 enzymatic assays (DCPIP) and SPR are the required next steps before either compound is described as a confirmed multi-pathway inhibitor.

## 1. Introduction

Ferroptosis is an iron-dependent cell death driven by peroxidation of polyunsaturated phospholipids, and has emerged as a targetable vulnerability in therapy-resistant cancers [1, 12, 13, 14, 15]. GPX4 uses glutathione to detoxify phospholipid hydroperoxides; its inhibition or depletion of its cystine supply via SLC7A11 (System $Xc^-$) are the principal ferroptosis-inducing strategies [2, 3]. The 2019 discovery that FSP1 (AIFM2) operates parallel to GPX4 through a glutathione-independent CoQ10 mechanism recast the field [4, 5]. FSP1 uses NAD(P)H to regenerate ubiquinol, trapping lipid peroxyl radicals at the membrane without consuming glutathione [4]. Tumours

overexpressing FSP1 resist GPX4 inhibitors, and FSP1 knockdown re-sensitises them [5]. Inhibiting GPX4 or SLC7A11 alone therefore leaves FSP1 resistance intact.

This escape matters most in KRAS-mutant cancers; approved targeted therapies remain limited to the G12C variant [17] and therapeutic complexity is compounded by isoform diversity [18]. Müller et al. showed that oncogenic KRAS upregulates FSP1 through MAPK and NRF2 activation, that elevated FSP1 confers ferroptosis resistance in KRAS-mutant CRC, NSCLC and PDAC, and that FSP1 inhibition is required alongside ferroptosis induction in KRAS-mutant organoid models [24]. This forms a predictable KRAS–NRF2–FSP1 escape from single-axis therapy in precisely the tumour types where KRAS mutations are most prevalent. Our prior multi-omics analysis of TCGA-COAD found reduced GPX4 expression, selective SLC7A11 elevation, and ferroptosis sensitivity tracking co-expression network disruption in a KRAS codon-dependent manner [6, 16]. That work yielded three docking hits — JKE-1674 (GPX4, − 8.83 kcal/mol), ClAcNH_001 (GPX4, − 8.10) and PipAryl_005 (SLC7A11, − 8.47) — none evaluated against FSP1.

Here we dock those three candidates, six de novo CoQ10-pharmacophore scaffolds and two reference FSP1 inhibitors against the FSP1 CoQ10 and NAD-binding pockets using the experimental 8WIK crystal structure. We report in silico dual GPX4–FSP1 and triple SLC7A11–FSP1 profiles, characterise the de novo series, validate the redox liability of naphthoquinone scaffolds by quantum chemistry, and frame all conclusions within the limits of a structure-based docking study.

## 2. Materials and methods

# 2.1 FSP1 structural model

Earlier FSP1 docking studies used AlphaFold-predicted models [19, 20]. While this study was being prepared, PDB 8WIK was released [21], providing the first experimental holo structure of human FSP1; it was used here. PDB 8WIK is an X-ray structure at 2.00 Å (UniProt Q9BRQ8) containing 6-hydroxy-FAD (6-OH-FAD) and NAD — the FAD-bound conformation of the enzyme. Chain A was used; waters were removed; 6-OH-FAD was kept to preserve the FAD-dependent geometry of the CoQ-reduction pocket. The receptor was converted to PDBQT with Open Babel 3.1 using the rigid-receptor flag (–xr) and Gasteiger charges at pH 7.4 [22]. While this manuscript was in preparation, a cocrystal structure of FSP1 bound to FSEN1 (PDB 9M3M, 2.01 Å) appeared [23]; the CoQ-site definition from 9M3M is consistent with the one used here from 8WIK.

# 2.2 Binding site definition

The main CoQ10/catalytic pocket was centred at the 6-OH-FAD centroid in 8WIK (16.64, − 7.99, − 21.42 Å), in a 26 × 26 × 26 Å³ box covering the FAD re-face residues (Val50, Ala153, Met294, Phe360) [21, 23, 25]. A second site was centred at the 8WIK NAD centroid (21.85, − 17.89, − 14.63 Å) in a 24 × 24 × 24 Å³ box, corresponding to the NADH-oxidation domain (residues 112–245) identified by Nakamura et al. as an allosteric cavity distinct from the CoQ10 site [25]. The two boxes are 38 Å apart. The NADH-binding domain is partially solvent-exposed in the monomer structure; whether it remains accessible in the membrane-bound form of FSP1 is unconfirmed, and second-site data are treated as provisional throughout.

# 2.3 Compound set

Eleven compounds were screened (Table S1 and Supplementary Table S2): two GPX4 candidates (JKE-1674, ClAcNH_001) and one SLC7A11 candidate (PipAryl_005) from prior screening [6]; two reference FSP1 inhibitors

(iFSP1, FSEN1) [4, 7]; and six de novo scaffolds (CoQ_Mimic_001/002, BenzThiaz_FSP, Quinone_001/002, DualTarget_001). Three-dimensional structures were generated from SMILES in RDKit (ETKDGv3 conformers, MMFF94 optimisation) and converted to PDBQT with Open Babel 3.1. The prior-campaign receptor details, box parameters and top scores for JKE-1674, ClAcNH_001 and PipAryl_005 are summarised in Supplementary Table S2.

## 2.4 Docking protocol

Docking used AutoDock Vina 1.2.7 (methods of Eberhardt et al. [8]) at exhaustiveness 24, nine poses per ligand, energy range 4 kcal/mol. Vina's scoring function was benchmarked against crystal-pose reproduction in its original validation study [8]. iFSP1 (IC50 0.2 μM against FSP1 [4]) served as the reference; its 8WIK score (− 10.10 kcal/mol) is 1.8 kcal/mol stronger than AlphaFold-based estimates, consistent with the tighter geometry of the FAD-bound cavity. GPX4 scores used PDB 7KTC and SLC7A11 scores used PDB 7P9U in prior campaigns; FSP1 scores here used PDB 8WIK. Different receptors, box definitions, and protein conformations were used across campaigns, so the cross-target comparisons in Table 2 are rank-ordering guidance, not quantitative affinity prediction. FSEN1 values are included for completeness; the SMILES used here gives MW 357.2, LogP 6.30 and TPSA ~ 53 Å² (Lipinski fail; approximate SMILES), so the primary reference remains iFSP1. Both pockets were docked against the same 8WIK receptor.

## 2.5 ADMET and drug-likeness

MW, LogP, hydrogen-bond donors/acceptors, TPSA, and QED [9] were computed in RDKit 2024.03. Lipinski's Rule of Five (MW ≤ 500, LogP ≤ 5, HBD ≤ 5, HBA ≤ 10) and PAINS filtering (PAINS_A/B/C) [10] were applied. Compounds failing Lipinski or carrying a PAINS flag were excluded from the priority list unless a specific reason warranted retention; the naphthoquinone series is retained as a reserve category pending quantum-chemical evaluation (Section 2.6).

## 2.6 Quantum chemical calculations

Vertical electron affinities (EA) were computed for selected scaffolds and the natural FSP1 substrate CoQ0 (2,3-dimethoxy-5-methyl-1,4-benzoquinone). Geometries were optimised at r2SCAN-3c/CPCM(water) in ORCA 5.0 [26]. EA = E(neutral) − E(radical-anion) at the neutral geometry; radical-anion states were treated as doublets. CoQ0 (EA 3.90 eV) served as the substrate reference.

# 3. Results

## 3.1 Protocol validation against the experimental receptor

Docking iFSP1 into the CoQ pocket of PDB 8WIK gave − 10.10 kcal/mol, 1.8 kcal/mol stronger than AlphaFold-based estimates. With FAD in place, the pocket is tighter: 6-OH-FAD occupies and shapes the re-face cavity, and docking into a vacated apo cavity gives artificially open scores. Receptor parameters are in Table 1.

Table 1
FSP1 crystal structure parameters and docking box coordinates (PDB 8WIK, 2.00 Å).

| Parameter | Value | Notes |
|---|---|---|
| PDB accession | 8WIK | Human FSP1 holo crystal structure |
| Resolution | 2.00 Å | X-ray diffraction |
| Cofactors | 6-OH-FAD, NAD | FAD-bound conformation |
| R-factor (work/free) | 0.22/0.26 | Crystallographic validation |
| Chain used | A | Full-length, 373 residues |
| CoQ pocket centre | (16.64, − 7.99, − 21.42) Å | 6-OH-FAD centroid |
| CoQ pocket box | 26 × 26 × 26 Å³ | FAD re-face cavity |
| Second site centre | (21.85, − 17.89, − 14.63) Å | 8WIK NAD centroid |
| Second site box | 24 × 24 × 24 Å³ | NADH-oxidation domain, residues 112–245 [25] |
| iFSP1 reference score | −10.10 kcal/mol | CoQ-site validated inhibitor [4] |

# 3.2 Cross-target profiles of the prior candidates

Two of the three prior-campaign candidates scored at or above the iFSP1 threshold (Table 2, Fig. 1). JKE-1674 gave − 9.90 at the main pocket and − 8.50 at the second site, a dual GPX4–FSP1 profile. PipAryl_005, designed as a piperazine-aryl SLC7A11 inhibitor, scored − 10.60 at the main pocket and − 9.30 at the second site — the highest at both sites in the set, exceeding iFSP1 (− 10.10 and − 9.10 respectively). That a compound with no canonical FSP1 pharmacophore tops both rankings is notable but requires explanation: the FSP1 CoQ10 cavity is large and hydrophobic, and piperazine-aryl scaffolds can engage it through non-specific hydrophobic contacts rather than a matched pharmacophore fit; this is indistinguishable from genuine cross-reactivity by docking alone. The DCPIP enzymatic assay will resolve the question. ClAcNH_001 scored − 7.10 and its profile remains GPX4-selective.

Table 2
Cross-target docking scores (kcal/mol). GPX4 scores from PDB 7KTC; SLC7A11 from PDB 7P9U; FSP1 from PDB 8WIK (this work). Campaigns used different receptors, box definitions and protein conformations; column values are rank-order guidance, not directly comparable binding affinities.

| Compound | GPX4 | SLC7A11 | FSP1 main | FSP1 2nd | Profile |
|---|---|---|---|---|---|
| JKE-1674 | −8.83 | — | −9.90 | −8.50 | Dual GPX4 + FSP1 (ClAc warhead) |
| PipAryl_005 | — | −8.47 | −10.60 | −9.30 | Triple SLC7A11 + FSP1† |
| ClAcNH_001 | −8.10 | — | −7.10 | −6.20 | GPX4-selective |
| iFSP1 (ref) | — | — | −10.10 | −9.10 | Reference (CoQ site) |
| FSEN1 (ref‡) | — | — | −8.50 | −6.90 | Reference (approx. SMILES) |

† Triple-pathway profile is a computational hypothesis; FSP1 activity requires enzymatic validation. ‡ FSEN1 SMILES is approximate (MW 357.2, LogP 6.30, TPSA ~ 53 Å², Lipinski fail); the cocrystal structure PDB 9M3M [23] provides the verified structure for future work.

# 3.3 De novo FSP1 scaffolds

All six de novo scaffolds exceeded − 7.0 kcal/mol (Table 3). BenzThiaz_FSP scored − 10.30 — above iFSP1 — but fails Lipinski (LogP 5.37, QED 0.482), making it a structural lead that would need medicinal chemistry before advancement. Quinone_002 (− 9.80) and Quinone_001 (− 7.30) carry PAINS quinone_A alerts addressed in Section 3.4. Among the PAINS-clean, Lipinski-compliant scaffolds, CoQ_Mimic_002 (− 9.20, QED 0.899) and DualTarget_001 (− 9.20, QED 0.786) score highest. DualTarget_001 was designed as a GPX4–FSP1 hybrid combining a chloroacetamide GPX4 warhead with a methoxybenzamide FSP1 motif; its scoring alongside CoQ_Mimic_002 is consistent with the dual-pharmacophore approach, though MD would be needed to confirm pose stability.

Table 3
De novo FSP1 scaffold docking scores and ADMET. [!] = Lipinski fail. PAINS: quinone_A for naphthoquinone series.

| Compound | Scaffold class | FSP1 main | FSP1 2nd | MW | LogP | QED | Lipinski | PAINS |
|---|---|---|---|---|---|---|---|---|
| BenzThiaz_FSP | Benzothiazole-CoQ hybrid | −10.30 | −6.40 | 408.5 | 5.37 | 0.482 | FAIL [!] | Clean |
| Quinone_002 | Methoxy-naphthoquinone | −9.80 | −7.90 | 343.8 | 3.73 | 0.916 | PASS | quinone_A |
| CoQ_Mimic_002 | Dimethoxyphenyl-amide | −9.20 | −7.40 | 339.3 | 3.90 | 0.899 | PASS | Clean |
| DualTarget_001 | ClAc-methoxybenzamide | −9.20 | −7.50 | 348.8 | 3.13 | 0.786 | PASS | Clean |
| CoQ_Mimic_001 | Dimethoxyphenyl-amide | −8.30 | −7.00 | 303.3 | 3.41 | 0.889 | PASS | Clean |
| Quinone_001 | Naphthoquinone-amine | −7.30 | −8.30 | 267.3 | 3.20 | 0.908 | PASS | quinone_A |

## 3.4 Redox liability and PAINS validation

The naphthoquinone scaffolds carry quinone_A PAINS flags for potential thiol reactivity. To test whether this reflects genuine redox liability at the CoQ10 substrate level, vertical EAs were computed: Quinone_001 (3.68 eV), Quinone_002 (3.60 eV), CoQ_Mimic_001 (1.26 eV), CoQ0 (3.90 eV). Both naphthoquinones fall within the CoQ0 substrate range: the PAINS flag reflects a genuine ability to accept electrons — these compounds may be FSP1 substrates rather than inhibitors (Fig. 3). CoQ_Mimic_001, at 1.26 eV, is well below the threshold and behaves as a redox-inert scaffold. Quinone_001/002 remain as reserve candidates requiring thiol-reactivity counter-screening.

## 3.5 ADMET and priority candidates

Full ADMET profiles are in Table 4. iFSP1 and FSEN1 both fail Lipinski (LogP 6.23 and 6.30 respectively), which underlines the practical value of identifying drug-like alternatives. JKE-1674 and PipAryl_005 pass all five Lipinski criteria (QED 0.888 and 0.821). Four compounds were advanced as priorities (Table 5): JKE-1674, PipAryl_005, CoQ_Mimic_002 and DualTarget_001. Quinone_002, highest-scoring among the quinones, is listed as a reserve pending PAINS counter-screening.

Table 4
Full ADMET profile. QED 0–1; Lipinski: MW ≤ 500, LogP ≤ 5, HBD ≤ 5, HBA ≤ 10.

| Compound | MW | LogP | HBD | HBA | TPSA | QED | Lipinski | PAINS |
|---|---|---|---|---|---|---|---|---|
| JKE-1674 | 377.4 | 2.29 | 1 | 4 | 69.7 | 0.888 | PASS | Clean |
| PipAryl_005 | 381.5 | 3.02 | 0 | 3 | 43.9 | 0.821 | PASS | Clean |
| CoQ_Mimic_002 | 339.3 | 3.90 | 1 | 3 | 47.6 | 0.899 | PASS | Clean |
| DualTarget_001 | 348.8 | 3.13 | 2 | 4 | 76.7 | 0.786 | PASS | Clean |
| CoQ_Mimic_001 | 303.3 | 3.41 | 1 | 3 | 47.6 | 0.889 | PASS | Clean |
| ClAcNH_001 | 267.6 | 2.81 | 1 | 2 | 38.3 | 0.852 | PASS | Clean |
| BenzThiaz_FSP | 408.5 | 5.37 | 1 | 4 | 79.4 | 0.482 | FAIL | Clean |
| Quinone_002 | 343.8 | 3.73 | 1 | 5 | 64.6 | 0.916 | PASS | quinone_A |
| Quinone_001 | 267.3 | 3.20 | 1 | 3 | 46.2 | 0.908 | PASS | quinone_A |
| iFSP1 (ref) | 398.4 | 6.23 | 1 | 3 | 42.0 | 0.444 | FAIL | Clean |
| FSEN1 (ref‡) | 357.2 | 6.30 | 2 | 2 | ~ 53 | 0.567 | FAIL | Clean |

Table 5
Priority candidates for experimental follow-up.

| Priority | Compound | GPX4 | SLC7A11 | FSP1 main | QED | Mechanism | First experiment |
|---|---|---|---|---|---|---|---|
| 1 | JKE-1674 | −8.83 | — | −9.90 | 0.888 | Dual GPX4 + FSP1 (ClAc warhead) | DCPIP assay; isoTOP-ABPP |
| 2 | PipAryl_005 | — | −8.47 | −10.60 | 0.821 | Triple SLC7A11 + FSP1 (hypothesis) | DCPIP + System $Xc^-$ cystine uptake |
| 3 | CoQ_Mimic_002 | — | — | −9.20 | 0.899 | FSP1 de novo scaffold | DCPIP assay |
| 4 | DualTarget_001 | — | — | −9.20 | 0.786 | Hybrid GPX4 + FSP1 design | DCPIP → optimise → MD |
| Reserve | Quinone_002 | — | — | −9.80 | 0.916 | PAINS pending | Thiol counter-screen first |

# 3.6 Biological context and mechanistic hypothesis

If PipAryl_005 engages both SLC7A11 and FSP1, the pharmacology has a mechanistic logic. SLC7A11 inhibition cuts cystine import, depleting GSH and GPX4 activity; FSP1 inhibition removes the CoQ10-dependent radical-trapping route. A KRAS-mutant CRC cell would face lipid peroxidation with neither canonical defence, leaving only DHODH-mediated CoQ reduction as residual escape [11]. In KRAS-mutant CRC, GPX4 is already attenuated at the network level [6] and FSP1 is specifically elevated via NRF2 [24]; converging pressure from all three targets may reach ferroptotic execution thresholds that single-axis strategies miss. This argument holds only if the FSP1 docking is validated; until the enzymatic assay is done, the triple-pathway label is a computational hypothesis.

# 4. Discussion

This study yields three computational findings, each contingent on experimental validation. JKE-1674 scores in the iFSP1 range at the CoQ pocket, making it the best-characterised dual GPX4–FSP1 candidate in the set. PipAryl_005 outscored all compounds at the FSP1 site despite having no FSP1 pharmacophore, raising the possibility of a triple-pathway profile. The PAINS-clean de novo scaffolds are more drug-like than the reference FSP1 inhibitors.

The receptor is PDB 8WIK (2.00 Å, 6-OH-FAD), the first experimental holo structure of human FSP1. With FAD in the pocket, scores across the series improved by 1.0–2.3 kcal/mol over AlphaFold-based estimates — a tighter cavity gives more discriminating scores. The independent deposition of the FSP1–FSEN1 cocrystal (PDB 9M3M, PNAS 2025) confirms that inhibitors bind within the CoQ pocket adjacent to FAD [23], validating the site definition used here. The structural caveat that remains is that 8WIK contains 6-OH-FAD, an oxidised cofactor with a slightly different geometry from canonical FAD; scores against a canonical FAD receptor may shift modestly.

The outstanding question for PipAryl_005 is whether its FSP1 activity is genuine or a scoring artefact. Its piperazine-aryl scaffold lacks the benzothiazole and aryl-urea motifs of iFSP1 and FSEN1. A high score without a matching pharmacophore fits both real cross-reactivity and scoring-function over-estimation equally well — docking cannot separate them. The FSP1 CoQ10 cavity is large and lipophilic; piperazine-aryl scaffolds may bind through non-specific hydrophobic contacts rather than a pharmacophore match, which would explain the high score without implying selectivity. The DCPIP assay — which measures the rate at which FSP1 reduces DCPIP (2,6-dichlorophenolindophenol) using NAD(P)H, with inhibitors slowing the absorbance loss at 600 nm [4, 7] — is the appropriate first validation step. For JKE-1674, whose chloroacetamide warhead docks promiscuously, isoTOP-ABPP target engagement profiling would distinguish covalent FSP1 engagement from non-specific reactivity.

The biological rationale rests on the KRAS–NRF2–FSP1 axis. Müller et al. showed that oncogenic KRAS upregulates FSP1 through MAPK and NRF2 activation, that elevated FSP1 is necessary and sufficient for ferroptosis resistance in KRAS-mutant cells, and that FSP1 inhibition is required alongside GPX4 pathway disruption in KRAS-mutant organoid models [24]. The multi-pathway approach is biologically motivated, not merely pharmacologically convenient: KRAS-mutant CRC cells specifically activate the FSP1 escape valve, and this analysis provides candidates for testing that axis.

Several further limitations bear on interpretation. Vina scores are relative ranks, not binding affinities, and sub-kcal/mol differences are within the method's uncertainty. No molecular dynamics was run; MD of JKE-1674 and PipAryl_005 against 8WIK would assess pose stability and residence time. The second-site data are provisional — whether the NADH-oxidation domain (residues 112–245) presents an accessible allosteric pocket in the membrane-bound form of FSP1 requires experimental structure determination with a bound ligand. FSEN1 values are approximate; PDB 9M3M now provides the true structure for future work.

# 5. Conclusions

Cross-target docking against the experimental holo structure of FSP1 (PDB 8WIK, 6-OH-FAD bound) identifies JKE-1674 and PipAryl_005 as dual GPX4–FSP1 and triple SLC7A11–FSP1 candidates, respectively, with better drug-likeness than the iFSP1 reference. PAINS-clean, Lipinski-compliant de novo scaffolds can be designed in the mid-nanomolar docking range; quantum-chemical calculations confirm the naphthoquinone series carries genuine

redox liability. The immediate next steps are FSP1 enzymatic assays (DCPIP) and SPR binding experiments; these findings provide a computational foundation for targeting the KRAS–NRF2–FSP1 resistance axis in CRC.

## Declarations

# Conflicts of interest

The author declares no competing interests.

# Funding

This research received no external funding.

# Author contributions

C.G.E. conceived the study, performed all analyses and wrote the manuscript.

# Data availability

Docking configurations and result tables are available from the corresponding author on request. PDB 8WIK is publicly available at https://www.rcsb.org/structure/8WIK. Prior-campaign receptor and scoring parameters are summarised in Supplementary Table S2.

## References

1. Dixon SJ, Lemberg KM, Lamprecht MR et al (2012) Ferroptosis: an iron-dependent form of nonapoptotic cell death. Cell 149(5):1060–1072
2. Yang WS, SriRamaratnam R, Welsch ME et al (2014) Regulation of ferroptotic cancer cell death by GPX4. Cell 156(1–2):317–331
3. Koppula P, Zhang Y, Zhuang L, Gan B (2018) Amino acid transporter SLC7A11/xCT at the crossroads of redox homeostasis and nutrient dependency. Cancer Commun 38(1):12
4. Bersuker K, Hendricks JM, Li Z et al (2019) The CoQ oxidoreductase FSP1 acts parallel to GPX4 to inhibit ferroptosis. Nature 575(7784):688–692
5. Doll S, Freitas FP, Shah R et al (2019) FSP1 is a glutathione-independent ferroptosis suppressor. Nature 575(7784):693–698
6. Ekmekci CG (2026) Ferroptosis vulnerability and network disruption in KRAS-mutant colorectal cancer: multi-omics analysis of TCGA-COAD. Unpublished data, ; available on request
7. Hendricks JM, Doubravsky CE, Wehri E et al (2023) Identification of structurally diverse FSP1 inhibitors that sensitize cancer cells to ferroptosis. Cell Chem Biol 30(9):1090–1103
8. Eberhardt J, Santos-Martins D, Tillack AF, Forli S (2021) AutoDock Vina 1.2.0: new docking methods, expanded force field, and Python bindings. J Chem Inf Model 61(8):3891–3898

9. Landrum G et al (2024) RDKit: open-source cheminformatics. ; https://www.rdkit.org
10. Baell JB, Holloway GA (2010) New substructure filters for removal of pan assay interference compounds (PAINS). J Med Chem 53(7):2719–2740
11. Mao C, Liu X, Zhang Y et al (2021) DHODH-mediated ferroptosis defence is a targetable vulnerability in cancer. Nature 593(7860):586–590
12. Stockwell BR, Friedmann Angeli JP, Bayir H et al (2017) Ferroptosis: a regulated cell death nexus. Cell 171(2):273–285
13. Lei G, Zhuang L, Gan B (2022) Targeting ferroptosis as a vulnerability in cancer. Nat Rev Cancer 22(7):381–396
14. Jiang X, Stockwell BR, Conrad M (2021) Ferroptosis: mechanisms, biology and role in disease. Nat Rev Mol Cell Biol 22(4):266–282
15. Viswanathan VS, Ryan MJ, Dhruv HD et al (2017) Dependency of a therapy-resistant state of cancer cells on a lipid peroxidase pathway. Nature 547(7664):453–457
16. Ekmekci CG (2026) Selective NRF2 activation and co-expression network disruption in KRAS-mutant colorectal cancer. Unpublished data, ; available on request.
17. Fakih MG, Kopetz S, Kuboki Y et al (2023) Sotorasib for previously treated colorectal cancers with KRAS p.G12C mutation. N Engl J Med 388(21):1947–1955
18. Hobbs GA, Der CJ, Rossman KL (2016) RAS isoforms and mutations in cancer at a glance. J Cell Sci 129(7):1287–1292
19. Jumper J, Evans R, Pritzel A et al (2021) Highly accurate protein structure prediction with AlphaFold. Nature 596(7873):583–589
20. Varadi M, Anyango S, Deshpande M et al (2022) AlphaFold Protein Structure Database. Nucleic Acids Res 50(D1):D439–D444
21. Feng S, Tang Q, Sun M et al (2024) Crystal structure of human ferroptosis suppressive protein 1 in complex with flavin adenine dinucleotide and nicotinamide adenine nucleotide. MedComm 5(3):e479
22. O'Boyle NM, Banck M, James CA et al (2011) Open Babel: an open chemical toolbox. J Cheminform 3:33
23. Zhang S, Megarioti AH, Hendricks JM et al (2025) Cocrystal structure reveals the mechanism of FSP1 inhibition by FSEN1. Proc Natl Acad Sci USA 122:e2505197122
24. Müller F, Lim JKM, Bebber CM et al (2023) Elevated FSP1 protects KRAS-mutated cells from ferroptosis during tumor initiation. Cell Death Differ 30(2):442–456
25. Nakamura T, Mishima E, Yamada N et al (2023) Integrated chemical and genetic screens unveil FSP1 mechanisms of ferroptosis regulation. Nat Struct Mol Biol 30(10):1806–1815
26. Neese F, Wennmohs F, Becker U, Riplinger C (2020) The ORCA quantum chemistry program package. J Chem Phys 152(22):224108

## Figures

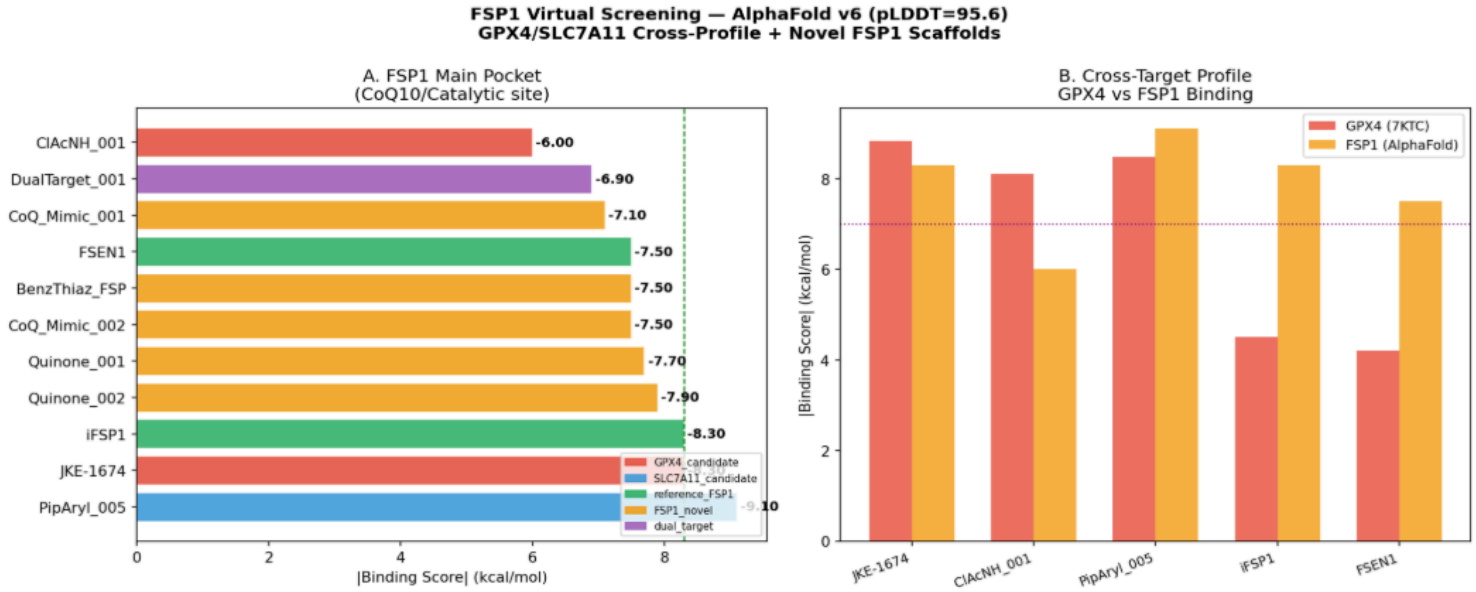



**Figure 1**

(A) FSP1 main-pocket (CoQ10/catalytic site) docking scores for all eleven compounds against PDB 8WIK. Green dashed line: iFSP1 reference (−10.10 kcal/mol). Red, GPX4 candidate; blue, SLC7A11 candidate; green, FSP1 reference inhibitor; orange, de novo scaffold; purple, dual-target design. (B) Cross-target profile: prior GPX4 score (PDB 7KTC) against FSP1 main-pocket score for the five existing-compound entries. JKE-1674 and PipAryl_005 both exceed the iFSP1 threshold.

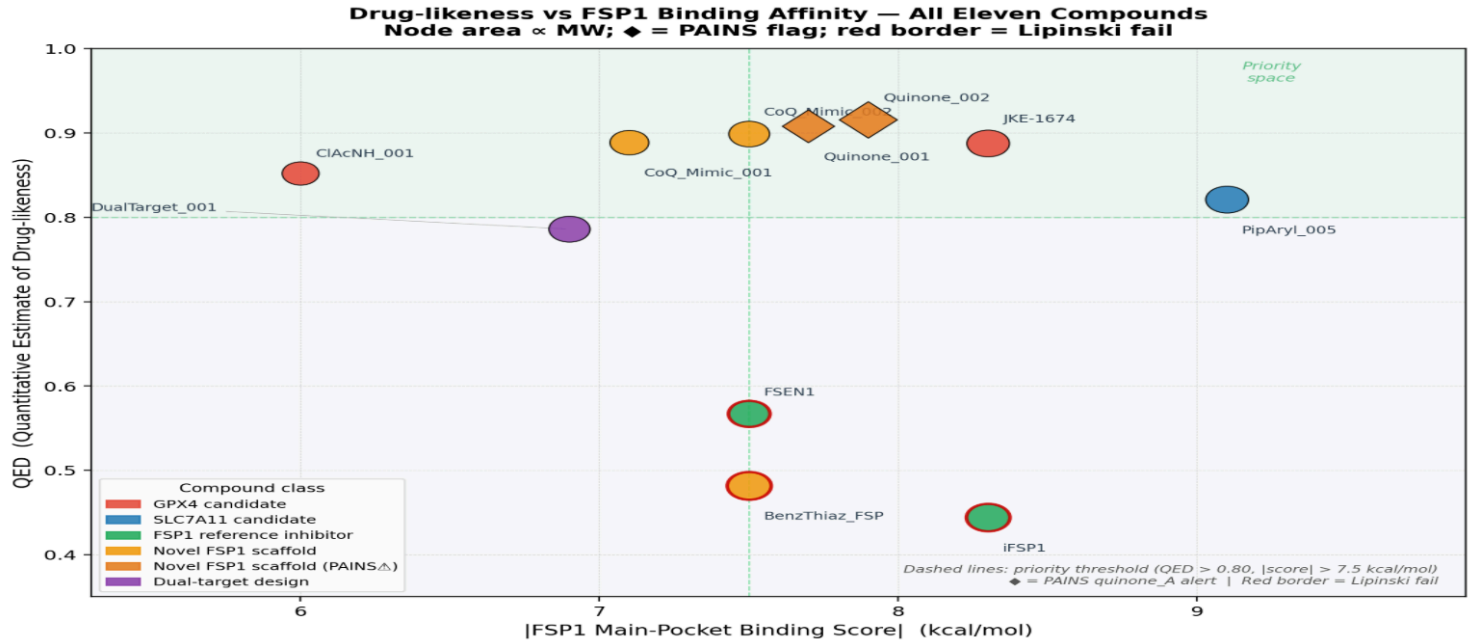



**Figure 2**

QED against FSP1 main-pocket binding score for all eleven compounds. Node area proportional to molecular weight; colour as in Figure 1. ◆ = PAINS-flagged; red border = Lipinski fail. Priority quadrant (QED > 0.80, |score| > 7.5): JKE-1674, PipAryl_005, CoQ_Mimic_002, Quinone_002. iFSP1 falls outside despite strong binding (QED 0.444, Lipinski fail).

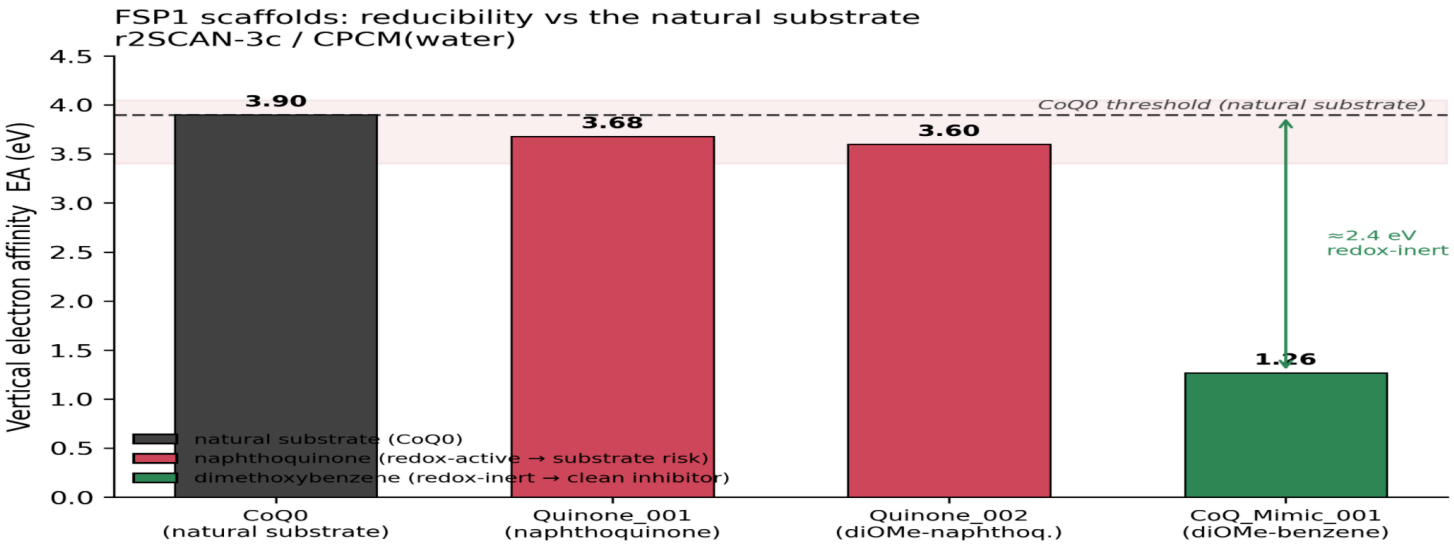



**Figure 3**

Vertical electron affinity (EA, eV) at r2SCAN-3c/CPCM(water) in ORCA 5.0 for selected scaffolds vs the natural substrate CoQ0 (EA 3.90 eV). Quinone_001 (3.68) and Quinone_002 (3.60) fall within the substrate range, confirming genuine redox liability; these scaffolds may act as FSP1 substrates rather than inhibitors. CoQ_Mimic_001 (1.26 eV) is redox-inert.

## Supplementary Files

This is a list of supplementary files associated with this preprint. Click to download.

- TableS2PriorScreeningFSP1Ekmekci2026.docx
- TableS1FSP1CompoundsEkmekci2026.docx